RESEARCH MEMORANDUM

LOW-SPEED MEASUREMENT OF TAIL CONTRIBUTION TO ROLLING STABILITY DERIVATIVES AND AIR-FLOW ANGULARITY AT THE TAIL FOR AN x-TAIL MODEL IN STEADY ROLL INCLUDING SOME EFFECTS OF WING-TIP STORES

By Donald R. Riley

Langley Aeronautical Laboratory
Langley Field, Va.

NATIONAL ADVISORY COMMITTEE
FOR AERONAUTICS

WASHINGTON

November 23, 1956
Declassified September 17, 1958

NACA RM L56I21

NATIONAL ADVISORY COMMITTEE FOR AERONAUTICS

RESEARCH MEMORANDUM

LOW-SPEED MEASUREMENT OF TAIL CONTRIBUTION TO ROLLING STABILITY DERIVATIVES AND AIR-FLOW ANGULARITY AT THE TAIL FOR AN X-TAIL MODEL IN STEADY ROLL INCLUDING SOME EFFECTS OF WING-TIP STORES

By Donald R. Riley

SUMMARY

An investigation has been made in the Langley stability tunnel to determine the combined effect of wing and wing-body interference on the contribution of an X-tail configuration to the low-speed rolling-stability derivatives of an airplane model having an unswept midwing and to indicate the change due to roll in the local flow angularity at a number of stations across the tail surfaces for one-half of the X-tail.

The results of the investigation indicated that adding the wing or the wing with tip stores to the fuselage-tail combination reduced the X-tail contribution to the damping in roll to about one-third of the available wing-off value for angles of attack of the model less than 10°. The air-flow angularity measurements made in the region of the tail for the wing-on configurations in steady roll at zero angle of attack indicated that the outboard half of each of the two surfaces surveyed produced damping in roll. For the inboard half of each of these surfaces, however, the angularity due to roll was such as to produce moments in the direction of roll. The two tail surfaces investigated were the upper right and the lower left when the model is viewed from the rear. Increasing the angle of attack shifted the spanwise location for the reversal in load due to roll in a direction outboard for the surface above the fuselage and inboard for the surface below the fuselage.

INTRODUCTION

Several investigations, such as references 1 and 2, have pointed out that for an airplane in steady roll the effect of wing interference at the vertical tail provides important changes in some of the rotary

stability derivatives, particularly for the yawing moment due to roll. These changes in the derivatives due to wing interference are the result of sidewash at the vertical tail that is caused by the antisymmetrical wing loading due to roll. Some work on missile configurations (refs. 3 and 4) has shown that the tail contribution to the damping in roll can be reduced as a result of adding a wing to a body-tail combination. Similar interference effects can be expected to occur on some present-day airplane designs that use unconventional arrangements of tail surfaces such as, for example, the V-tail and the X-tail. These interference effects are of especial interest for those airplanes having tail spans and tail areas that are large in comparison with those of the wing. For such configurations, a division of the load due to roll between the wing and tail would also be desirable for structural design purposes.

The present low-speed investigation was made to determine the combined effect of wing and wing-body interference on the tail contribution of an X-tailed airplane configuration in steady roll and to provide measurements of the change in the local flow angularity due to roll at a number of stations across the tail surfaces for one-half of the X-tail. The present investigation, in addition, includes the effect of adding external stores to the wing tips.

SYMBOLS

The force and moment data presented herein are in the form of standard coefficients which are referred to the stability system of axes with the origin located on the fuselage center line at the longitudinal position of the quarter chord of the wing mean aerodynamic chord. The positive directions of the force and moment coefficients, angles, and angular velocities are shown in figure 1. The coefficients and symbols are defined as follows:

C_L lift coefficient, $\frac{\text{Lift}}{qS_w}$

C_D drag coefficient, $\frac{\text{Drag}}{qS_w}$

C_Y lateral-force coefficient, $\frac{\text{Lateral force}}{qS_w}$

C_l rolling-moment coefficient, $\frac{\text{Rolling moment}}{qS_w b_w}$

C_m pitching-moment coefficient, $\frac{\text{Pitching moment}}{qS_w \bar{c}_w}$

C_n yawing-moment coefficient, $\frac{\text{Yawing moment}}{qS_w b_w}$

q dynamic pressure, $\frac{1}{2}\rho V^2$

V free-stream velocity

ρ mass density of air

A aspect ratio, b^2/S

b span, measured perpendicular to fuselage center line

S plan-form area

c chord, measured parallel to fuselage center line (see fig. 3)

$\bar{c}$ mean aerodynamic chord, $\frac{2}{S}\int_0^{b/2} c^2 dy$

y spanwise coordinate measured perpendicular to fuselage center line

l_t tail length, distance from quarter chord of wing mean aerodynamic chord to quarter chord of tail mean aerodynamic chord measured parallel to fuselage center line

α angle of attack of fuselage center line, deg

α_t local angle of attack of tail or local air-flow angle relative to tail chord at any spanwise station of tail measured in a plane perpendicular to surface, positive when producing positive lift on tail, radians

p rolling angular velocity

$\frac{pb_w}{2V}$ wing-tip helix angle, radians

$\frac{\partial \alpha_t}{\partial \frac{pb_w}{2V}}$ flow angularity derivative or rate of change of local angle of attack at station on tail with wing-tip helix angle

$$C_{Y_p} = \frac{\partial C_Y}{\partial \frac{pb_w}{2V}}$$

$$C_{n_p} = \frac{\partial C_n}{\partial \frac{pb_w}{2V}}$$

$$C_{l_p} = \frac{\partial C_l}{\partial \frac{pb_w}{2V}}$$

Subscripts:

w refers to wing

t refers to tail

The test configurations and the designations used in identifying the data on the figures are as follows:

F	fuselage
F + T	fuselage with X-tail
W + F	wing with fuselage
W + F + S	wing with fuselage and tip stores
W + F + T	wing with fuselage and X-tail
W + F + S + T	wing with fuselage, tip stores, and X-tail

APPARATUS AND MODEL

The tests were made in the 6-foot-diameter rolling-flow test section of the Langley stability tunnel. This test section is equipped with a motor-driven rotor located upstream of the model. When in operation, the rotor imparts a twist to the airstream such that a model mounted rigidly at the test location is in a field of flow similar to that which exists about an airplane in flight rolling about its longitudinal stability axis. (See ref. 5.)

The model used in the present investigation was designed to permit tests of the fuselage alone and in combination with the wing, the X-tail, or both. For the wing-on configuration, the model was tested with and without external stores mounted at the wing tips. A drawing of the complete model is presented as figure 2. A list of the geometric characteristics of the various component parts is given in table I. Details of the wing and tail profiles and a table of ordinates for the fuselage is presented as figure 3. A photograph of the complete model mounted in the tunnel is presented as figure 4.

For the tests the model was mounted on a single support strut which was shielded by a fairing of circular cross section. The forces and moments exerted on the model were measured by means of a six-component electromechanical balance. The flow angles in the region of the tail were measured by means of a 3/16-inch-diameter pitot-static yaw head tube which was mounted from the fuselage base. The pressure leads were permitted to trail downstream with the wind for a distance of about one wing span and were then brought through a $1\frac{3}{4}$-inch-diameter pipe spanning the tunnel jet.

Flow-angle measurements were obtained for only two of the four exposed tail surfaces. These two surfaces were the lower left and upper right when the model is viewed from the rear and have been designated herein as surfaces A and B, respectively. The measurements were made, of course, with the X-tail removed. At each spanwise test station, the axis of the yaw-head tube was alined with the tail chord and the orifices were oriented so that flow-angle measurements were obtained in a plane parallel to the fuselage center line and perpendicular to the tail-chord plane.

TESTS

The tests were made at a dynamic pressure of 39.7 pounds per square foot which corresponds to a Mach number of about 0.166 and a Reynolds number, based on the wing mean aerodynamic chord, of 1.1×10^6.

The fuselage alone and with the wing, X-tail, and tip-stores in various combinations was tested through an angle-of-attack range from -4° to 24° in straight flow and from -4° to 20° in rolling flow. All tests were made at an angle of sideslip of 0°. For the straight-flow tests $\left(\frac{pb_w}{2V} = 0\right)$, the lift, drag, and pitching moments were measured. The data obtained in rolling flow at several values of $\frac{pb_w}{2V}$ were used to obtain

the lateral-force, yawing-moment, and rolling-moment derivatives with respect to wing-tip helix angle. The test values of $\frac{pb_w}{2V}$ were ± 0.0137, ± 0.0274, and ± 0.0412.

For these values of $\frac{pb_w}{2V}$ and for a value of zero, the local angles of attack of the tail were measured by means of a yaw head tube. Data were recorded at 16 spanwise stations for one-half of the X-tail through an angle-of-attack range from -4° to 16° in increments of 2°. The spanwise stations corresponded to values of y from 3 to 10 inches at 1-inch intervals for both surface A and surface B. The measured values of α_t were plotted against wing-tip helix angle and values for the derivative $\frac{\partial \alpha_t}{\partial \frac{pb_w}{2V}}$ were obtained for each of the 16 spanwise stations for each angle of attack of the model.

CORRECTIONS

The angle of attack and the coefficients of drag, pitching moment, and rolling moment have been corrected for tunnel wall effects. The data are not corrected for blocking or support-strut interference since previous experience indicated these corrections to be small. In addition, no corrections were applied to the airstream angularity measurements at the tail to account for tunnel wall effects on the wing wake since it was felt that this effect on the flow-angularity derivative would be small.

RESULTS AND DISCUSSION

Static Longitudinal Characteristics

The lift, drag, and pitching-moment coefficients for the various model configurations with the wing on are presented in figure 5 and the corresponding data for the fuselage alone and with the X-tail are given as figure 6. The results for the wing-on configurations show that a small value of lift coefficient was obtained at $\alpha = 0^\circ$. Part of this value is due to the load carried on the wing as a result of the wing profile used and its orientation relative to the fuselage axis. (See figs. 2 and 3.) The lift results of figure 5, in addition, indicate that adding tip stores to either the wing-fuselage or to the wing-fuselage-tail combination increased the lift-curve slope of the

configuration by about 10 percent. The addition of tip stores also provided a small change in the slope of pitching-moment coefficient with angle of attack in the low angle-of-attack range. Some additional wind-tunnel information for a geometrically similar configuration in the Mach number range 0.50 to 0.92 showing the effects of propeller operation is available in reference 6.

Steady-Roll Characteristics

Tail contribution.- The variation of the steady rolling derivatives C_{Y_p}, C_{n_p}, and C_{l_p} with angle of attack for the various model configurations with the wing on are presented in figure 7. The corresponding data for the fuselage alone and fuselage-tail combination are presented in figure 8. The tail contributions due to steady roll for the various configurations are presented in figure 9 and were obtained by subtracting the values of the derivatives for the tail-off configuration from the corresponding tail-on configuration.

The wing-off tail contribution to the damping in roll shown in figure 9 is several times larger than that produced by a conventional vertical- and horizontal-tail group. This result is to be expected for the present X-tailed model because of the large values of the ratios of tail span to wing span $\left(\frac{b_t}{b_w} = 0.63\right)$ and total tail area to wing area $\left(\frac{S_t}{S_w} = 0.69\right)$.

Of particular interest in figure 9 are the differences between the curves for the wing-on and wing-off configurations. These differences are the combined effect of wing and wing-body interference and represent the change in the effectiveness of the tail caused by the addition of the wing to the fuselage-tail combination. The largest differences in the low angle-of-attack range between wing-on and wing-off curves for the data in figure 9 were obtained for the damping in roll. The effect of adding the wing to the fuselage-tail combination on the X-tailed contribution to the damping in roll, in general, was to reduce (that is, C_{l_p} becomes less negative) the tail contribution to about one-third of the available wing-off values for angles of attack up to about 10°. In the low angle-of-attack range the addition of the wing provided no change in the lateral-force derivative but did indicate a change in C_{n_p}. This change corresponds, of course, to a rearward shift in the tail center of pressure. In general, these results appeared to apply whether the tip stores were on or off. There would appear to be some reservations concerning the actual magnitudes of the rearward center-of-pressure shift and the reductions in C_{l_p} indicated on figure 9 as a result of the scatter shown for the data in figures 7 and 8.

The results of reference 1 indicated that the effect of adding an unswept wing on the contribution of a vertical- and horizontal-tail group to the steady-roll derivatives was to provide a change in C_{Y_p} and C_{n_p} with a negligible change in C_{l_p}. For the present x-tailed model in the low angle-of-attack range the reduction in the tail contribution to C_{l_p} with no effect on C_{Y_p} due to the addition of the wing is attributed to the arrangement and size of the tail surfaces.

Effect of stores.- The primary effect of the stores, as would be expected, was on the wing contribution to the steady-roll derivatives. (See fig. 7.) The results indicated that adding tip stores to the wing-fuselage or wing-fuselage-tail combination provided a large increase in the damping in roll for angles of attack up to about 8°. In general, above about 8° to an angle of attack near maximum lift ($\alpha = 15°$), the magnitude of C_{l_p} with the stores on was less than the corresponding configuration with the stores off. Reference 7 indicates a similar trend due to stores of decreased damping in roll with an increase in angle of attack. The magnitude of the increase in C_{l_p} at $\alpha = 0°$ due to the addition of the stores expressed as a percentage of the value of the store-off configuration is in agreement with the value predicted by the expression in reference 8. The addition of the wing-tip stores also provided rather large increases in the slope of the lateral force derivative with α at low angles of attack for configurations with and without the x-tail and little change in the yawing-moment derivative C_{n_p}.

Angularity Measurements

The reduction in the tail contribution to the damping in roll with little change in the lateral-force derivative when the wing or wing-tip-store combination was added to the fuselage-tail configuration (fig. 9) is indicative of a change in the spanwise load distribution across the tail. Therefore, a flow-angle survey across the positions occupied by two surfaces of the x-tail was made for the fuselage-alone, the wing-fuselage, and the wing-fuselage-store configurations. The results are presented in figures 10 and 11 in the form of $\frac{\partial \alpha_t}{\partial \frac{pb_w}{2V}}$ which is the rate of change of the local angle of attack of any station on the tail with wing-tip helix angle. Figure 10 gives the variation of the local tail angle (or flow angularity) derivative with model angle of attack for each of the stations investigated and figure 11 shows a cross plot of

the spanwise distribution of $\frac{\partial \alpha_t}{\partial \frac{pb_w}{2V}}$ across the tail surfaces for angles of attack of 0°, 4°, 8°, and 12°.

In addition to the measured data, a curve representing the variation of $\frac{\partial \alpha_t}{\partial \frac{pb_w}{2V}}$ that would be expected in perfect rolling flow at the location of the yaw head if the model were removed is shown in figures 10 and 11. The curve was included mainly for comparison with the fuselage-alone data. A comparison of the two curves at the large values of y should provide an indication of the overall accuracy of the test data. The difference between the curves would, of course, be the combined result of a number of factors; however, the main contributors would be the accuracy of the flow-angle measurements and the accuracy with which the rotor equipment at the entrance to the test section reproduced the rolling flow over the area surveyed. The comparison would be expected to be valid only at the large values of y since, for the inboard stations tested, such as values of y of 3 or 4 inches, for example, the fuselage and model support strut would be expected to modify the results. When all factors are considered, the agreement shown is reasonably good.

A comparison of results shown in figure 10 for wing-on and wing-off configurations at each spanwise station indicates that the effect on the flow-angularity derivative of adding the wing or wing-store combination to the fuselage is to provide about a constant change in the derivative (across the tail span) in the low angle-of-attack range. It should be pointed out that the local angle of attack of the tail α_t was defined as positive for both surface A and B when a positive lift component was produced. As a result, a positive value of the derivative for surface B is necessary to produce damping in roll, whereas a negative value of the derivative for damping in roll is necessary for surface A. In the low angle-of-attack range the data of figure 10 indicate that the effect of adding the wing changed the angularity distribution so as to reduce the damping in roll contributed at every spanwise station investigated. This fact is more apparent in figure 11 which presents the spanwise distribution of the flow-angularity derivative.

An examination of figure 11 shows that for the model at zero angle of attack a reversal in the sign of $\frac{\partial \alpha_t}{\partial \frac{pb_w}{2V}}$ occurred for the wing-on configurations over the inboard half of surfaces A and B. As the angle of attack of the model was increased, the spanwise position of this sign reversal shifted outboard for tail B until, at angles of attack of 12°

and above (see also fig. 10), almost the complete tail surface produced a moment about the body axis in the direction of roll. For surface A, however, increasing the angle of attack of the model shifted the spanwise location of the sign reversal on $\frac{\partial \alpha_t}{\partial \frac{pb_w}{2V}}$ inboard and at higher angles of attack eliminated the sign reversal completely. (See also fig. 10.) Of additional interest in figure 11 is the fact that, at $\alpha = 12^\circ$, the values of the angularity derivative for tail B over the inboard portion of the surface for the wing-on configuration reached magnitudes almost twice as large as the magnitudes of the flow-angle derivative that would be obtained at the tip of the wing. These large negative values appear to be associated with separated flow from the wing. For example, the data of figure 10 for the inboard portion of tail surface B indicate that a large change in the angularity derivative for wing-on values occurred at $\alpha = 10^\circ$. These changes were associated with abrupt negative shifts in the value of α_t at zero roll and large losses in dynamic pressure which indicate, of course, separated flow.

CONCLUSIONS

The results of an investigation to determine the combined effect of wing and wing-body interference on the tail contributions to the low-speed rolling stability derivatives of an X-tail model and to indicate the change in the flow-angularity distribution due to steady roll across the tail surfaces for one-half of the X-tail indicate the following conclusions:

1. The magnitude of the tail contribution to the damping in roll of the complete model was about a third of the available wing-off value for angles of attack less than 10°. In the low angle-of-attack range the addition of the wing provided no change in the tail contribution to the lateral-force derivative due to roll but indicated a rearward shift in the tail center of pressure. These results appeared to apply equally well for configurations with or without tip stores.

2. The spanwise distribution of air-flow angularity at the tail due to steady roll for the wing-on configurations at zero angle of attack indicated that the outboard half of each of the two surfaces investigated produced damping in roll whereas, for the inboard half, the air-flow angularity produced moments in the direction of roll. The two tail surfaces investigated were the lower left and upper right when the model is viewed from the rear.

3. Increasing the angle of attack for wing-on configurations in steady roll shifted the spanwise position for the sign reversal on the flow-angularity derivative in a direction inboard for the lower left tail surface and outboard for the upper right tail surface.

4. The addition of wing-tip stores to the wing-fuselage configuration with and without the X-tail increased the lift-curve slope, the damping in roll at low angles of attack, and the lateral-force derivative due to roll.

Langley Aeronautical Laboratory,
National Advisory Committee for Aeronautics,
Langley Field, Va., August 31, 1956.

REFERENCES

1. Letko, William, and Riley, Donald R.: Effect of an Unswept Wing on the Contribution of Unswept-Tail Configurations to the Low-Speed Static- and Rolling-Stability Derivatives of a Midwing Airplane Model. NACA TN 2175, 1950.

2. Michael, William H., Jr.: Analysis of the Effects of Wing Interference on the Tail Contributions to the Rolling Derivatives. NACA Rep. 1086, 1952. (Supersedes NACA TN 2332.)

3. Scherrer, Richard, and Dennis, David H.: Damping in Roll of a Missile Configuration With a Modified Triangular Wing and a Cruciform Tail at a Mach Number of 1.52. NACA RM A51A03, 1951.

4. Steinmetz, Harold F.: Wing-Body Interference Effects on the Tail Contribution to the Damping-in-Roll of Supersonic Missiles. Preprint No. 384, S.M.F. Fund Preprint, Inst. Aero. Sci., July 16-18, 1952.

5. MacLachlan, Robert, and Letko, William: Correlation of Two Experimental Methods of Determining the Rolling Characteristics of Unswept Wings. NACA TN 1309, 1947.

6. Sutton, Fred B., and Buell, Donald A.: The Effect of an Operating Propeller on the Aerodynamic Characteristics at High Subsonic Speeds of a Model of a Vertical-Rising Airplane Having an Unswept Wing of Aspect Ratio 3. NACA RM A52E06, 1954.

7. Murray, Harry E., and Wells, Evalyn G.: Wind-Tunnel Investigation of the Effect of Wing-Tip Fuel Tanks on Characteristics of Unswept Wings in Steady Roll. NACA TN 1317, 1947.

8. Campbell, John P., and McKinney, Marion O.: Summary of Methods for Calculating Dynamic Lateral Stability and Response and for Estimating Lateral Stability Derivatives. NACA Rep. 1098, 1952. (Supersedes NACA TN 2409.)

TABLE I.- GEOMETRIC CHARACTERISTICS OF THE MODEL

Fuselage:	
Length, in.	41.85
Fineness ratio	6.44
Wing:	
Aspect ratio	3.07
Taper ratio	0.33
Quarter-chord sweep angle, deg	5.66
Airfoil section	Modified flat plate
Airfoil section thickness, percent	Approximately 6
Area, sq in.	354.75
Span, in.	33.00
Mean aerodynamic chord, in.	11.65
One-half of the X-tail:	
Aspect ratio	3.55
Taper ratio	0.38
Quarter-chord sweep angle, deg	30.00
Airfoil section	Modified flat plate
Airfoil section thickness, percent	Approximately 6
Area, sq in.	121.68
Span, from tip to tip, in.	20.80
Mean aerodynamic chord	6.25
Tail length, l_t, in.	16.01
Store:	
Length, in.	16.80
Fineness ratio	9.34

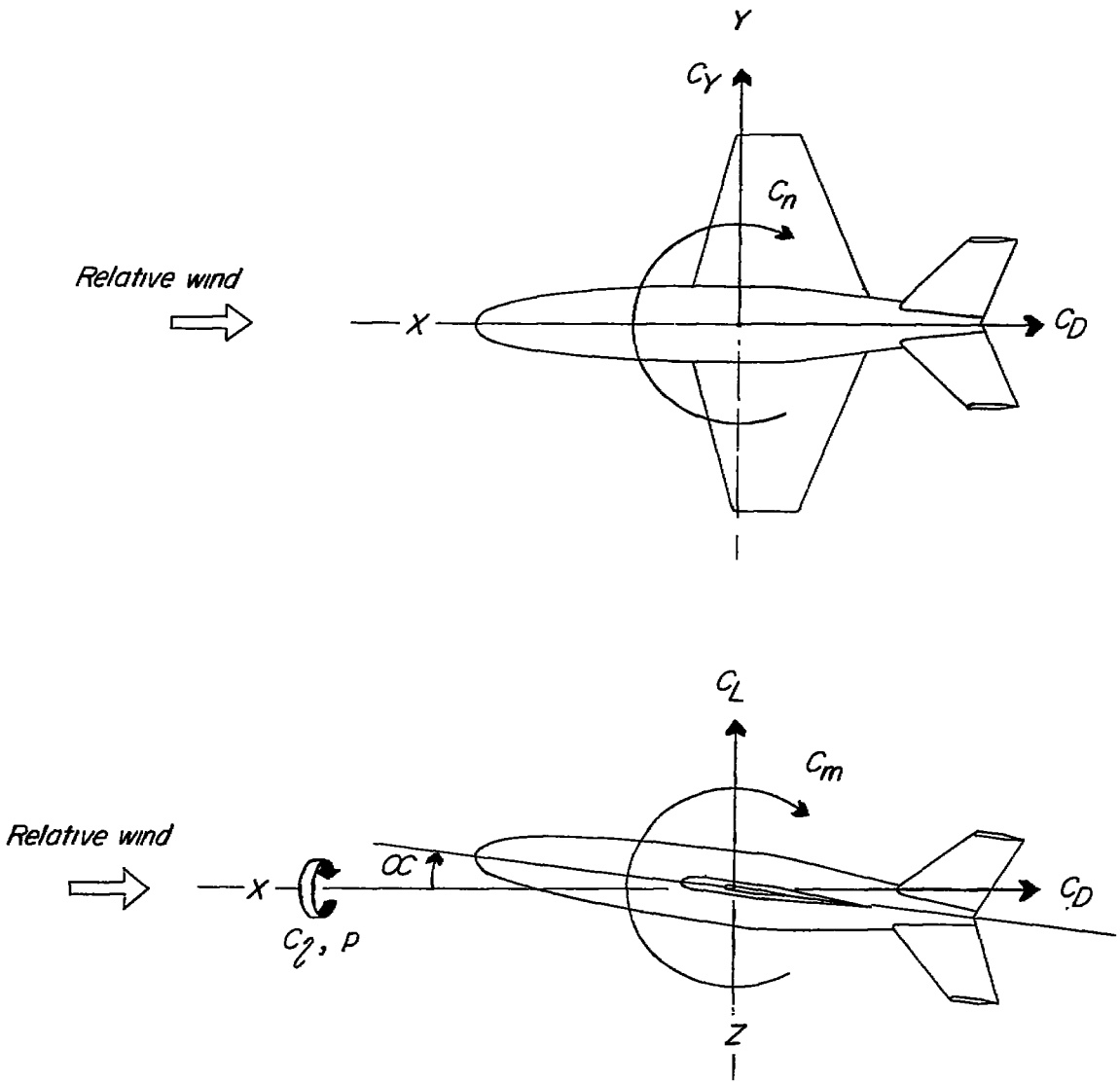

Figure 1.- System of axes used. Arrows indicate positive directions.

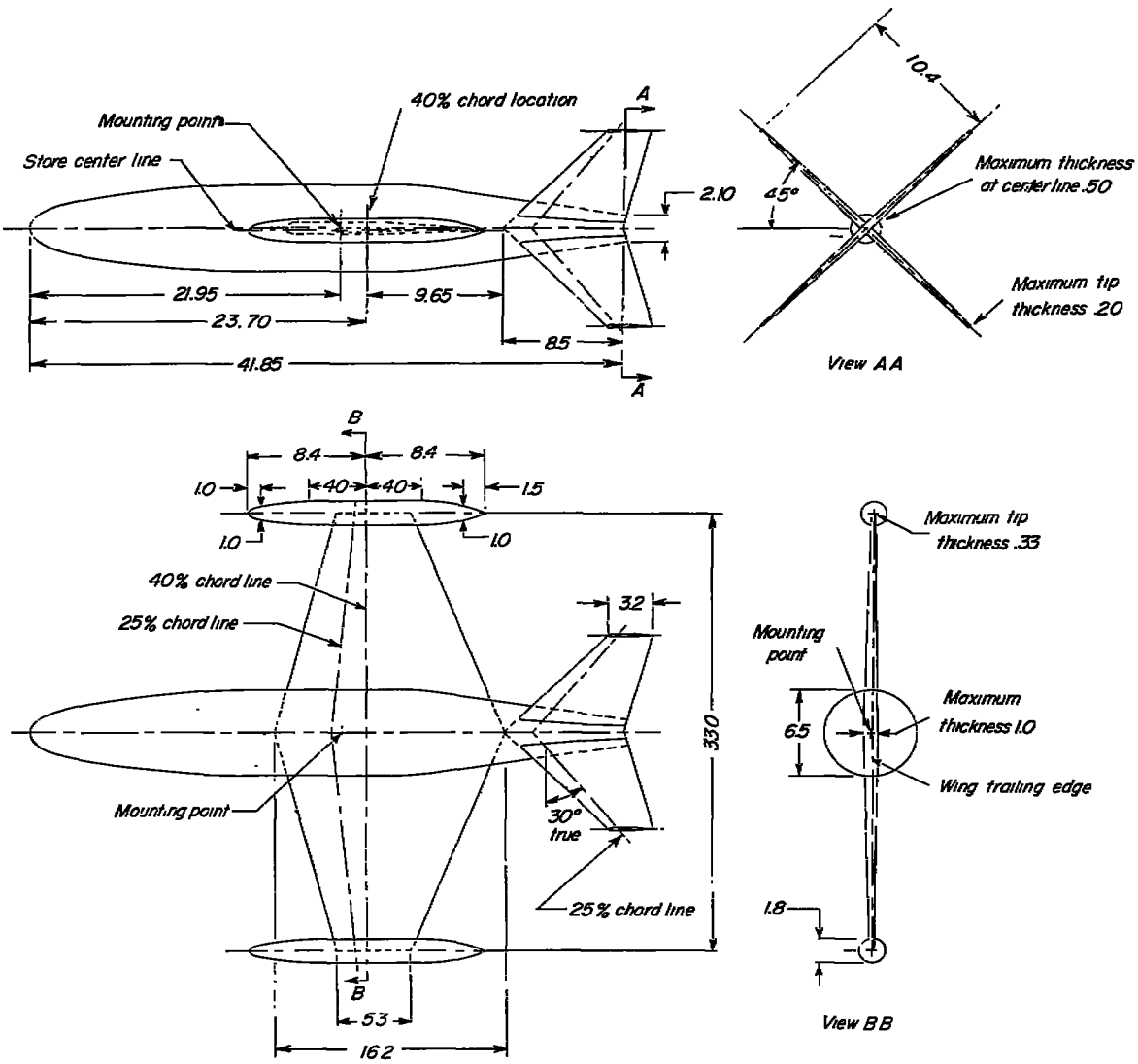

Figure 2.- A drawing of the complete X-tail model. All dimensions are in inches.

Profile of wing

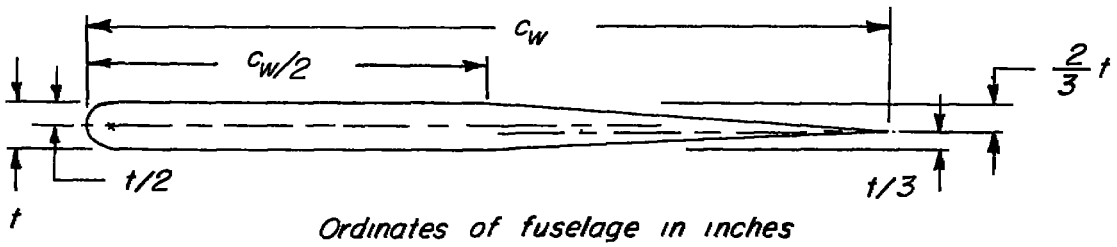

Ordinates of fuselage in inches

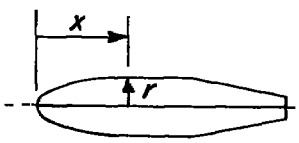

x	r	x	r
0	0	11.90	3.10
.02	.20	13.41	3.20
.09	.40	15.10	3.23
.38	.80	16.00	3.25
.62	1.00	26.00	3.25
.93	1.20	27.00	3.22
1.34	1.40	28.00	3.10
1.86	1.60	29.00	2.93
2.51	1.80	30.00	2.79
3.34	2.00	32.00	2.49
4.37	2.20	34.00	2.21
5.67	2.41	36.00	1.92
7.31	2.63	38.00	1.63
9.34	2.85	40.00	1.34
10.55	2.98	42.00	1.05

Profile of X tail

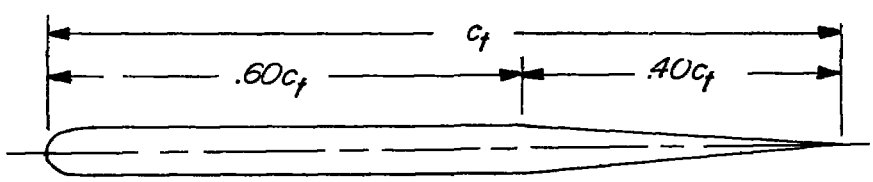

Figure 3.- Details of the wing and tail profiles and a table of ordinates for the fuselage.

L-75328

Figure 4.- Rear view of the X-tail model shown at a slight angle of sideslip in the 6-foot-diameter rolling-flow test section of the Langley stability tunnel.

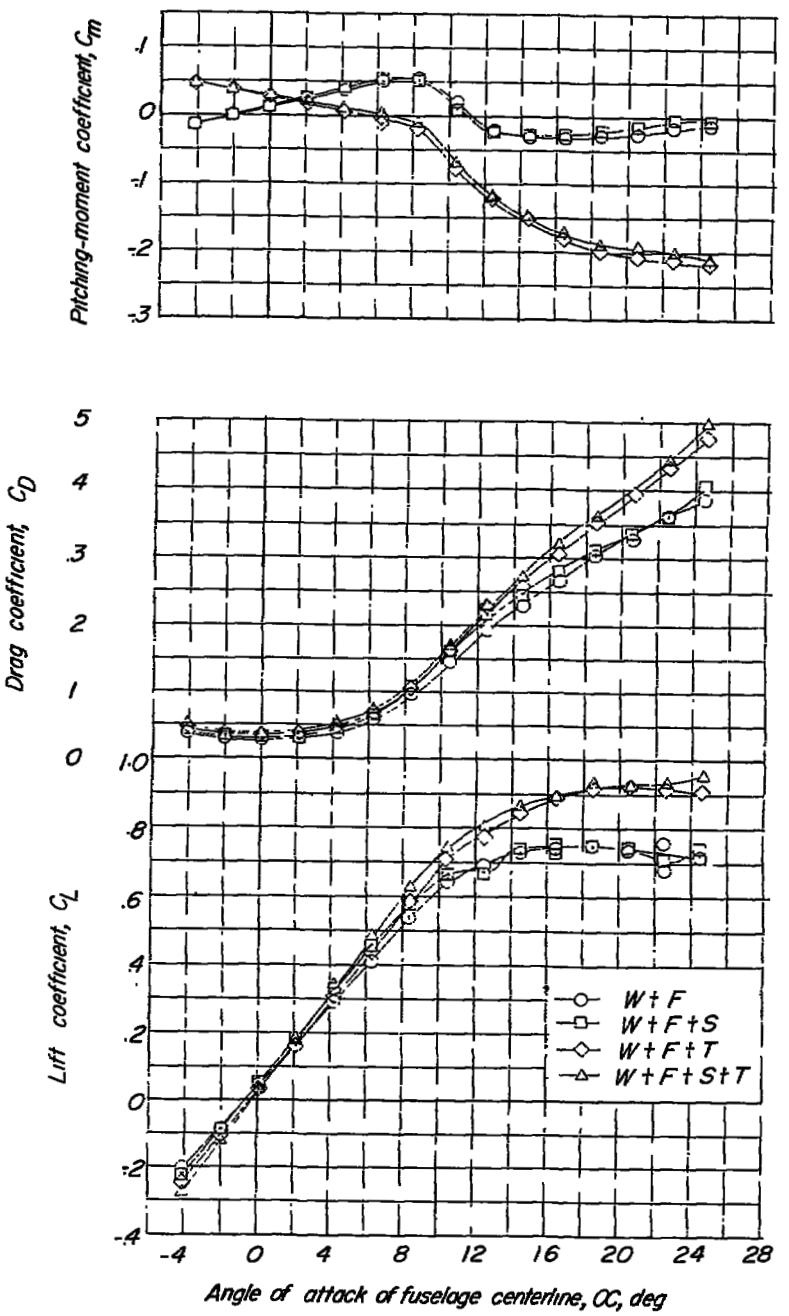

Figure 5.- The lift, drag, and pitching-moment characteristics for the wing-fuselage configuration with and without the wing-tip stores and X-tail.

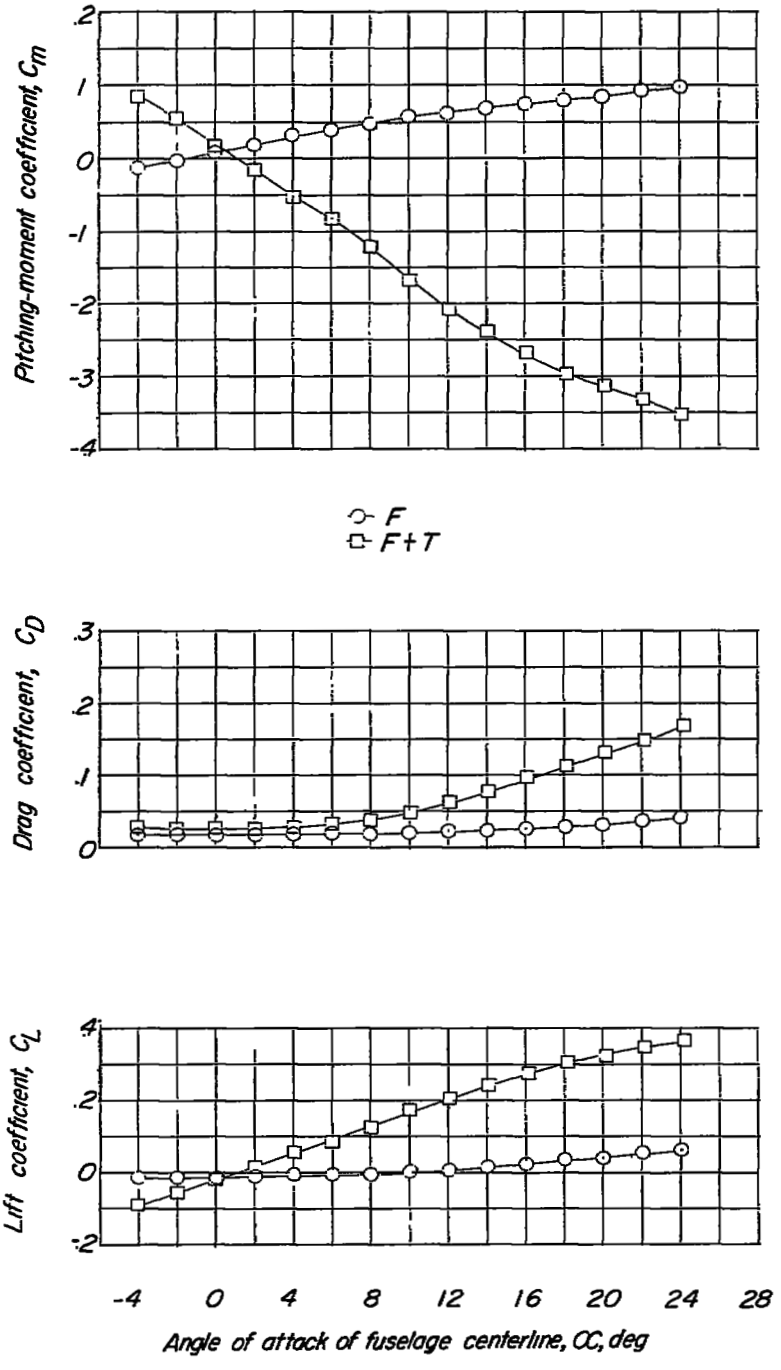

Figure 6.- The lift, drag, and pitching-moment characteristics for the fuselage alone and with the X-tail.

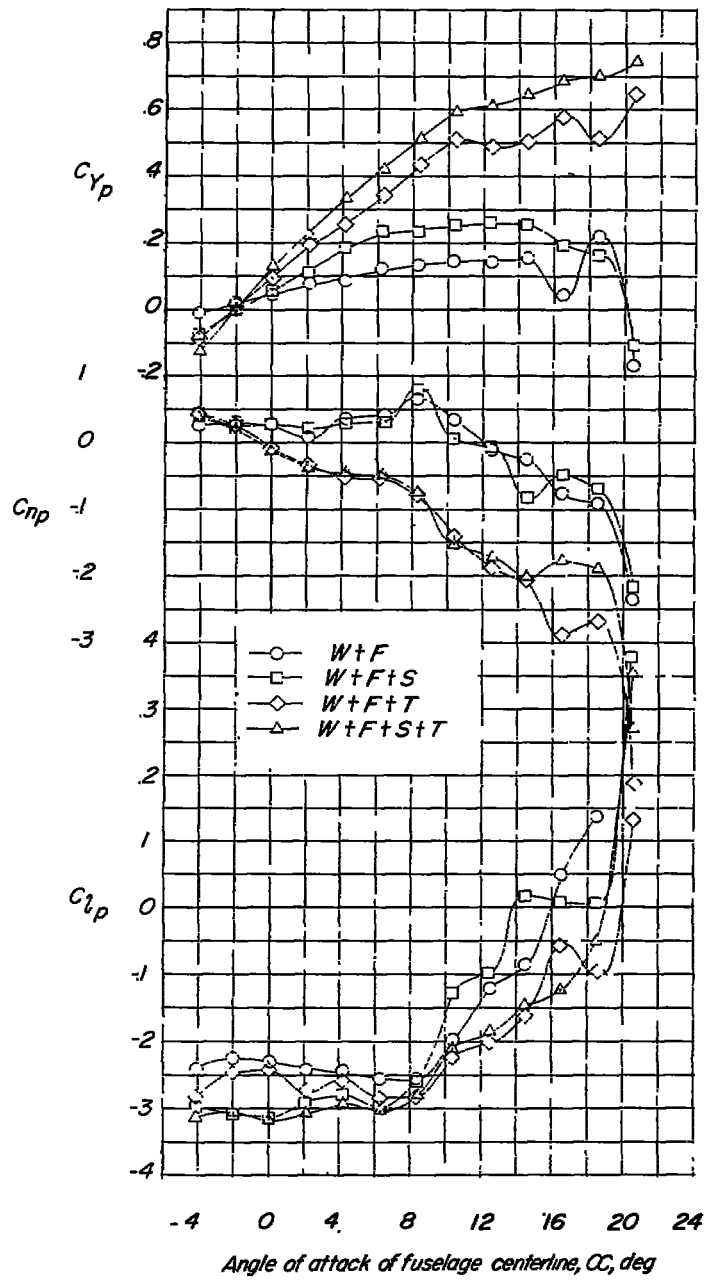

Figure 7.- Variation with angle of attack of C_{Y_p}, C_{n_p}, and C_{l_p} for the wing-fuselage combination with and without the wing-tip stores and X-tail.

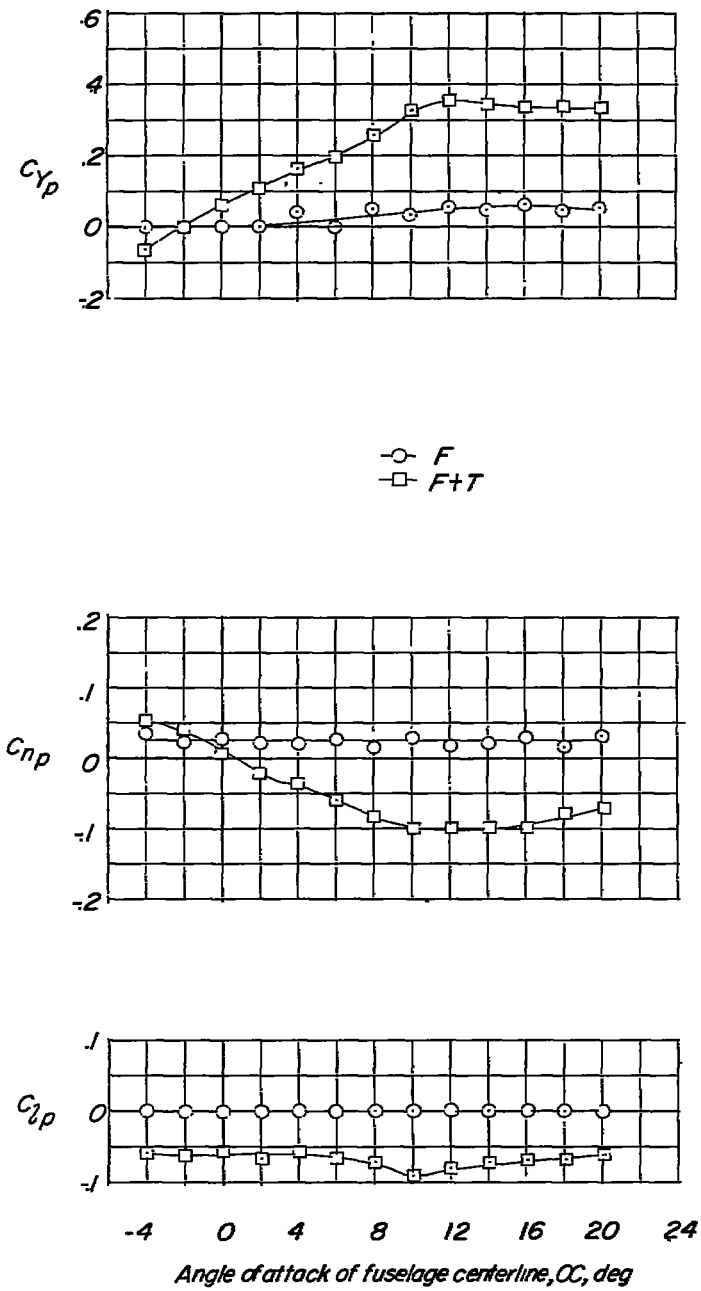

Figure 8.- Variation with angle of attack of C_{Y_p}, C_{n_p}, and C_{l_p} for the fuselage alone and with the X-tail.

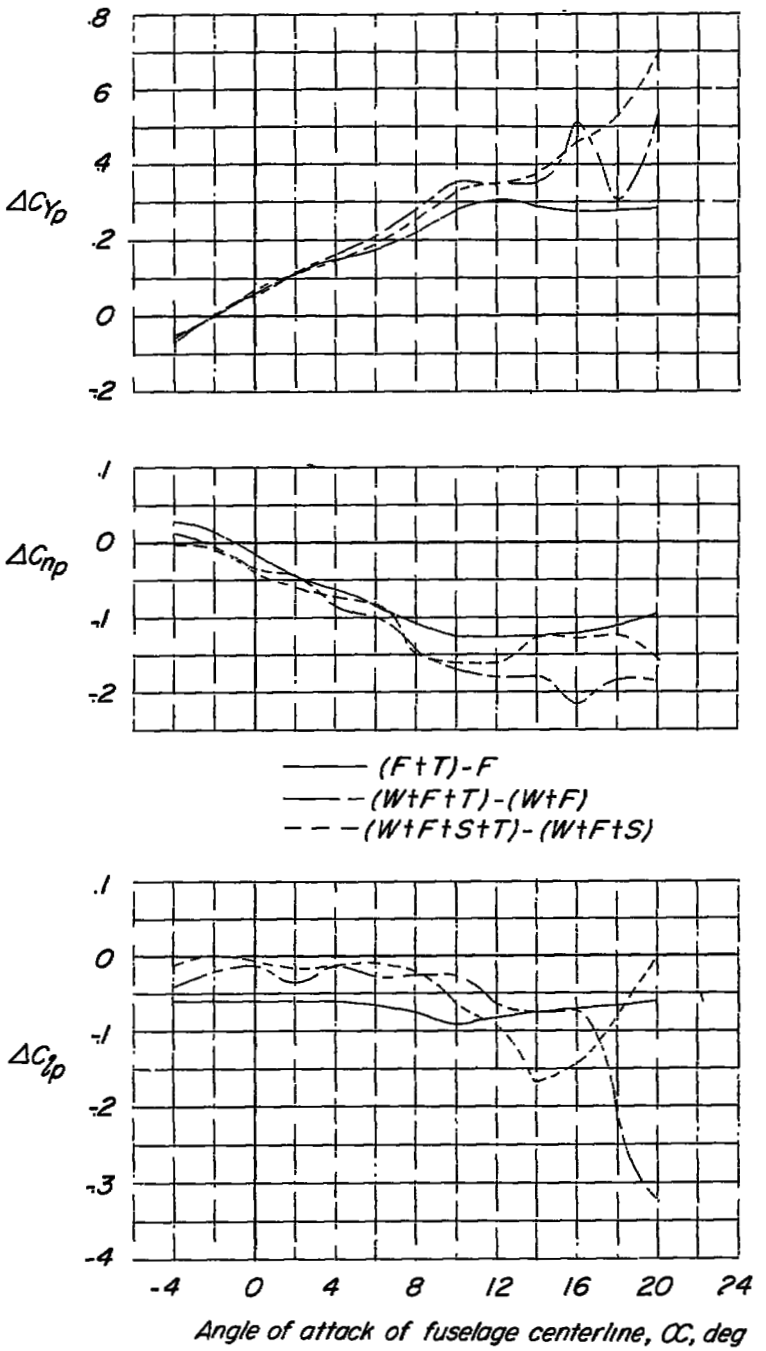

Figure 9.- Variation with angle of attack of the x-tail contribution to the rolling stability derivatives.

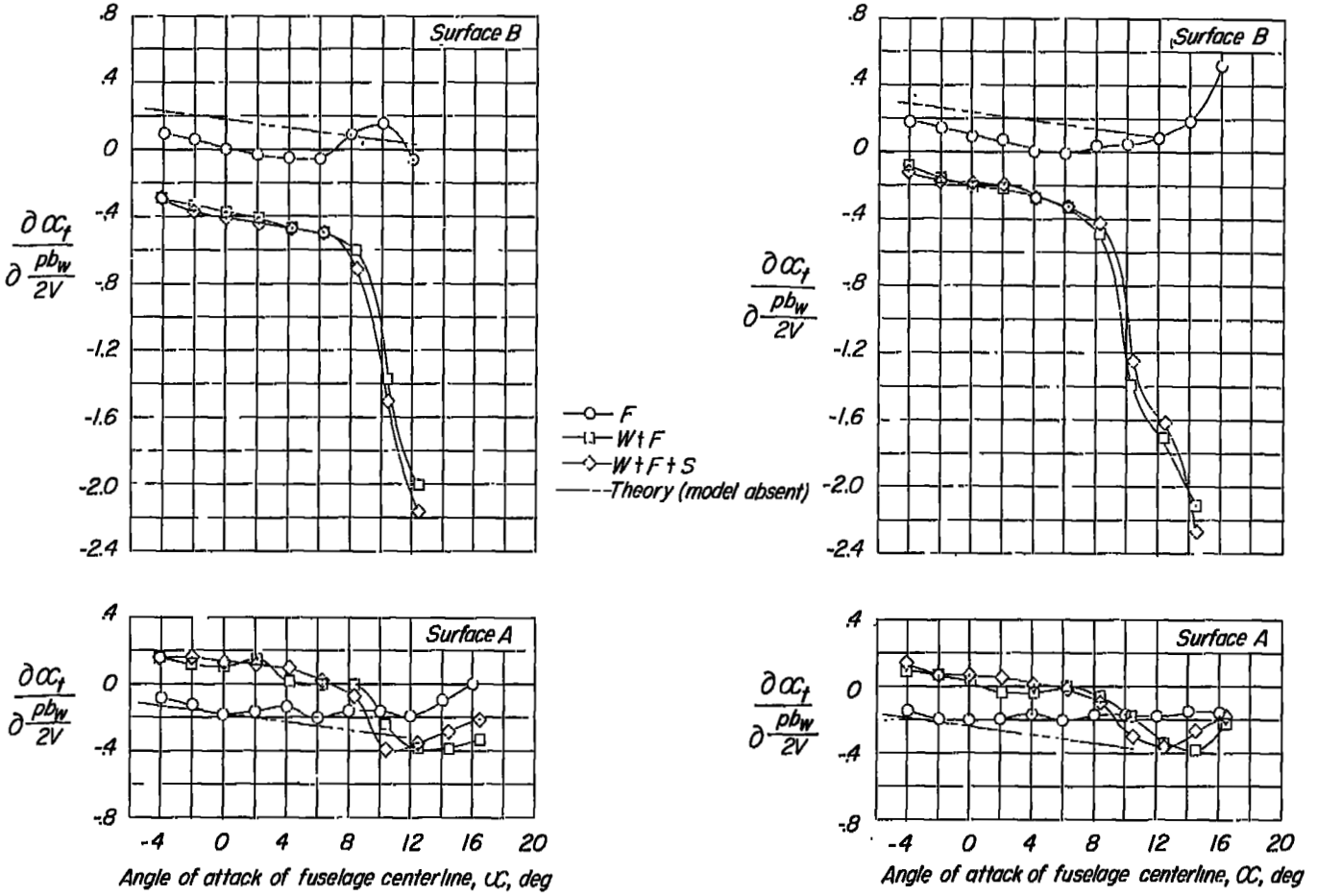

(a) Spanwise station, y = 3 inches.

(b) Spanwise station, y = 4 inches.

Figure 10.- Variation of the airstream angularity derivative at the tail $\frac{\partial \alpha_t}{\partial \frac{pb_w}{2V}}$ with model angle of attack for each of the spanwise stations investigated at tail surfaces A and B.

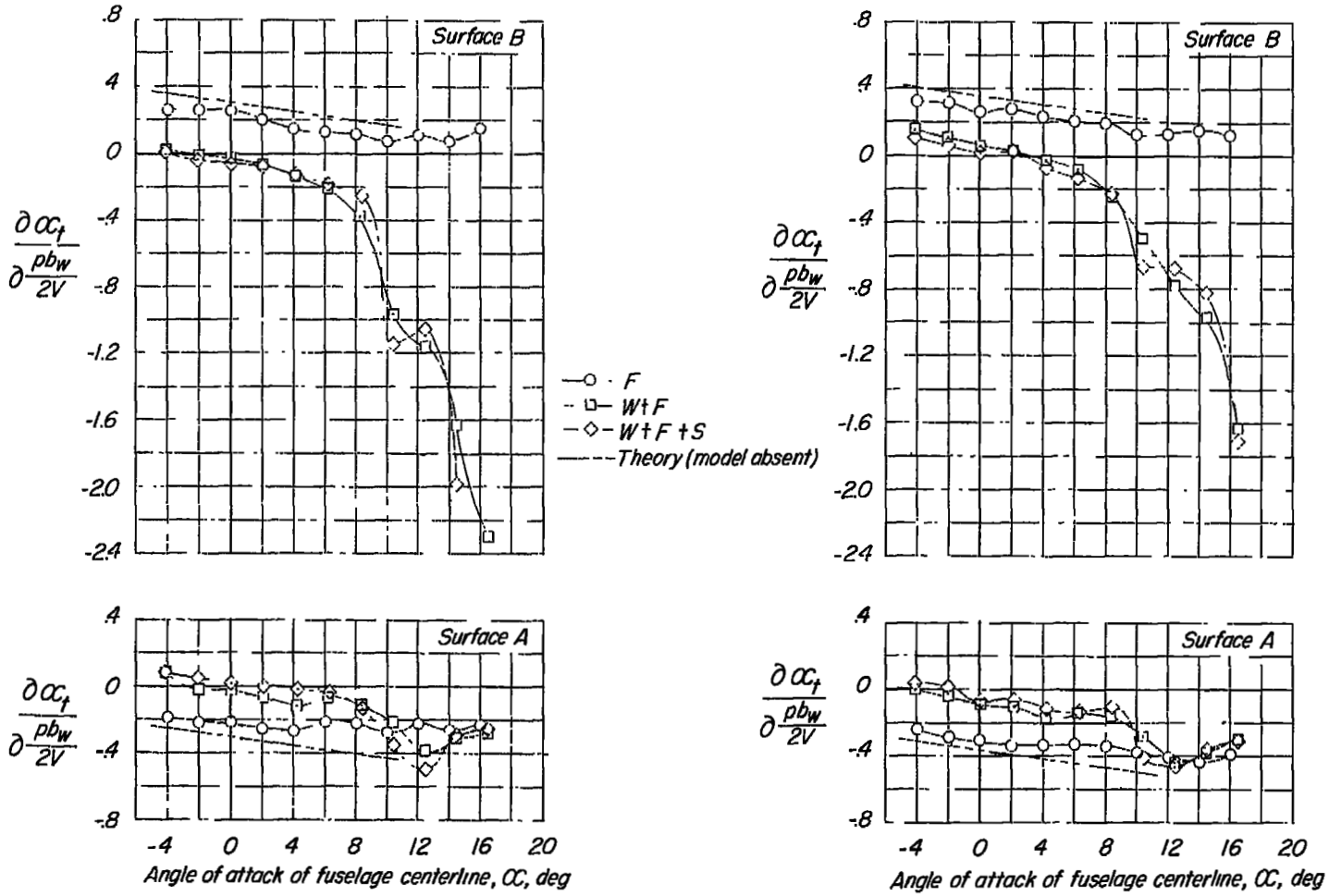

(c) Spanwise station, y = 5 inches.

(d) Spanwise station, y = 6 inches.

Figure 10.- Continued.

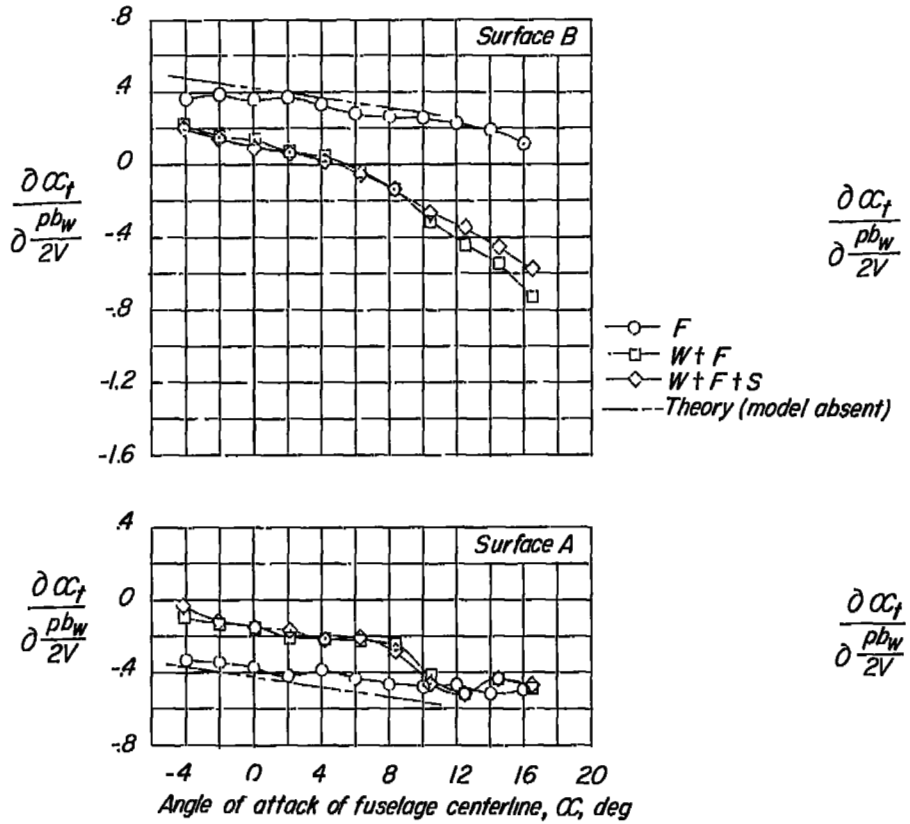

(e) Spanwise station, y = 7 inches.

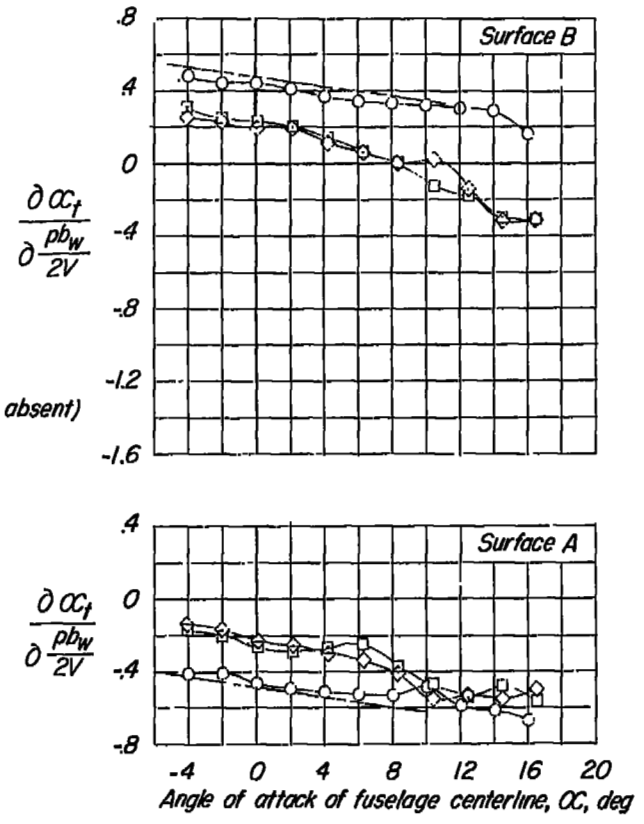

(f) Spanwise station, y = 8 inches.

Figure 10.- Continued.

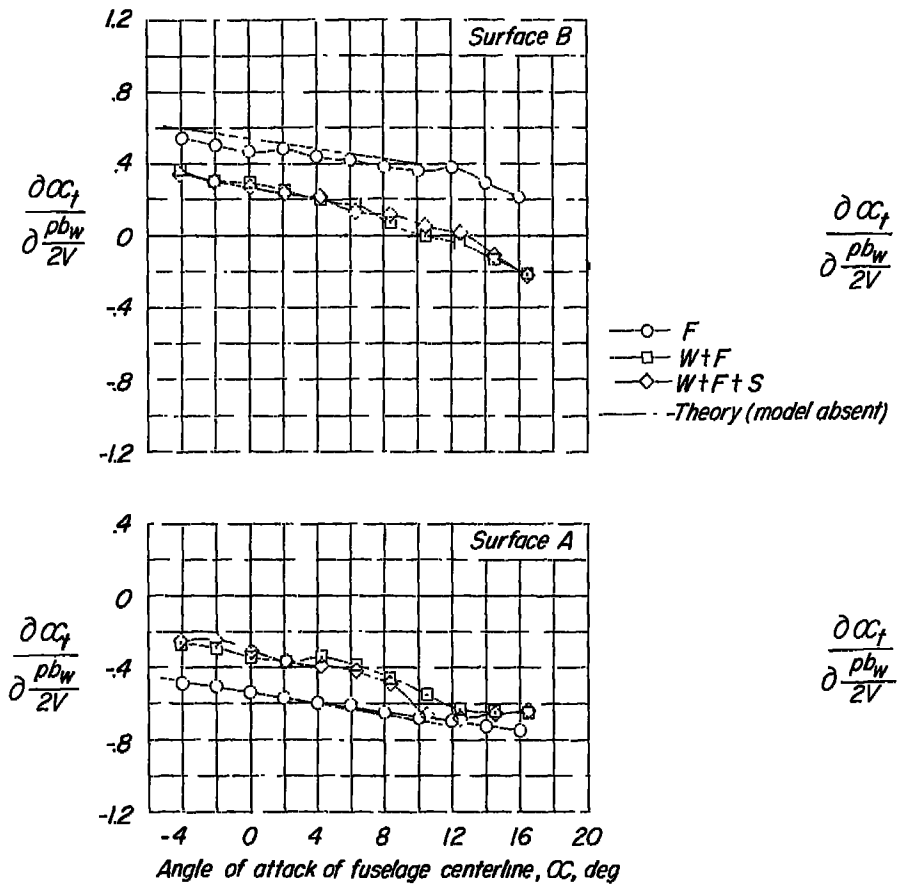

(g) Spanwise station, y = 9 inches.

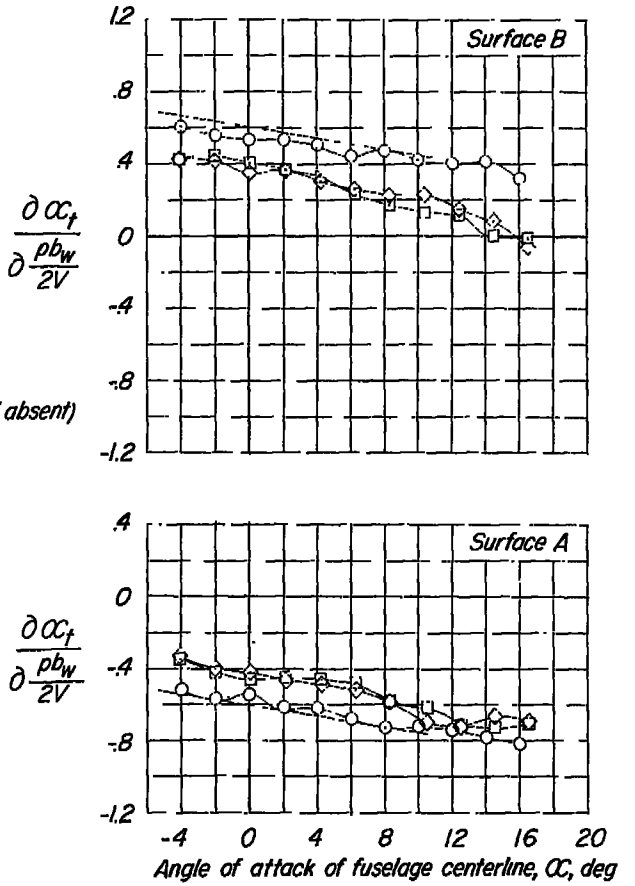

(h) Spanwise station, y = 10 inches.

Figure 10.- Concluded.

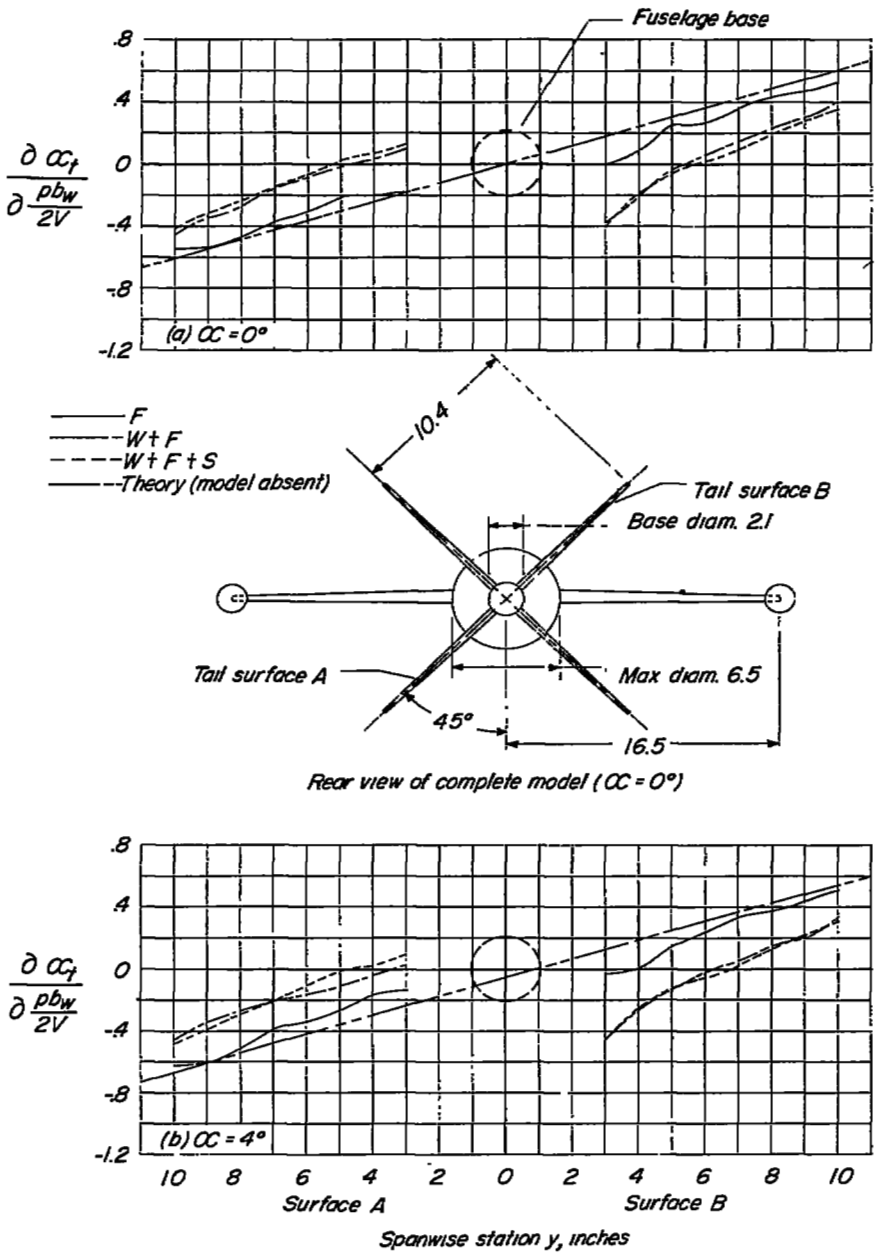

Figure 11.- Spanwise distributions of the airstream angularity derivative at the tail $\frac{\partial \alpha_t}{\partial \frac{pb_w}{2V}}$ for tail surfaces A and B at several angles of attack of the model.

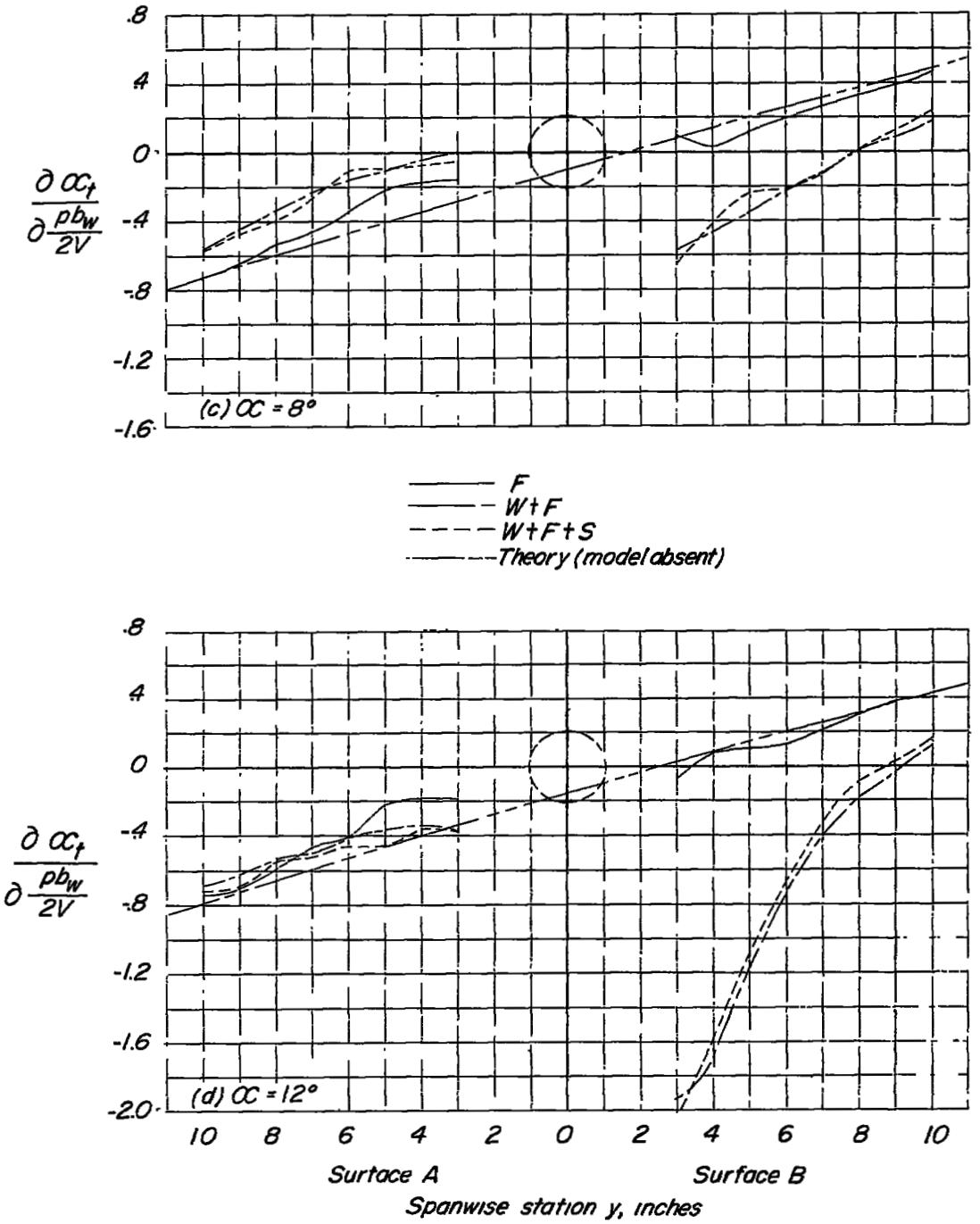

Figure 11.- Concluded.